Nano Research

Open Access

Research Article

Self-powered tactile sensor for real-time recognition of Morse code based on machine learning

Shenxing Tan[1,2,3,§], Yang Jiang[3,4,§], Xujiang Chao[5,§], Fei Liang[2], Ripeng Li[6], Tao Jiang[1,3,4] ✉, Hai-Dong Yu[2] ✉, and Zhong Lin Wang[1,3] ✉

[1] *Guangzhou Institute of Blue Energy, Guangzhou 510555, China*
[2] *Frontiers Science Center for Flexible Electronics, Xi'an Institute of Flexible Electronics (IFE), and Xi'an Institute of Biomedical Materials & Engineering, Northwestern Polytechnical University, Xi'an 710072, China*
[3] *Beijing Key Laboratory of Micro-Nano Energy and Sensor, Center for High-Entropy Energy and Systems, Beijing Institute of Nanoenergy and Nanosystems, Chinese Academy of Sciences, Beijing 101400, China*
[4] *School of Nanoscience and Engineering, University of Chinese Academy of Sciences, Beijing 100049, China*
[5] *School of Mechanical Engineering, Northwestern Polytechnical University, Xi'an 710072, China*
[6] *School of Computer Science (National Pilot Software Engineering School), Beijing University of Posts and Telecommunications, Beijing 100876, China*
[§] *Shenxing Tan, Yang Jiang, and Xujiang Chao contributed equally to this work.*

Cite this article: *Nano Research*, **2025**, *18*, 94907167. https://doi.org/10.26599/NR.2025.94907167

ABSTRACT: Developing lightweight, green, and flexible wearable electronics with high sensitivity and multifunctional sensing capabilities is of important significance in the field of outdoor sports, such as mountaineering, animal tracking and protection. This work proposes a silk fibroin fibers-based triboelectric nanogenerator (SF-TENG) to harvest tiny energy from human fingertip tapping and act as a self-powered tactile sensor. The SF-TENG adopts a green, efficient, and low-cost fabrication strategy, in which a breathable and electropositive silk fibroin fiber membrane and a silver conductive layer are prepared by electrostatic spinning and magnetron sputtering, and combined with a conductive cloth and a breathable tape to form a flexible sensor that can be attached to a human skin. The thin and soft portable TENG device, having a thickness of only 0.3 mm and a mass of 354 mg at the dimension of 4.5 cm × 4.5 cm, can generate a maximum power density of 1.0 mW·m^{-2}. Furthermore, the SF-TENG has excellent sensitivity of 1.767 mV·Pa^{-1} with good cyclic stability. The superior sensing characteristics provide new avenues for Morse code applications toward outdoor wearable autonomous communication. The proposed SF-TENG offers promising solutions in multi-scenario outdoor sport, human-machine interface interaction, and security systems.

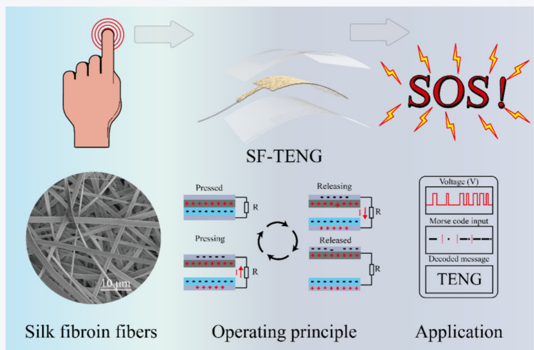

KEYWORDS: flexible electronics, triboelectric nanogenerator, silk fibroin, Morse code translation

1 Introduction

With the rapid development of the Internet of Things and the popularization of human-computer interaction technologies, there is an increasingly urgent need for portable and miniaturized electronic devices that are more stable, environmentally friendly, and efficient [1–5]. These devices have attracted much attention in communication equipment, personal security alarms, etc., due to their small and portable nature [6–10]. They provide a convenient means of daily communication and play an essential role in emergencies, providing users with security and emergency help functions. Among these applications, Morse code is highly regarded for its excellent performance in low-bandwidth environments and is considered as an efficient and reliable means of emergency communication. These practical applications highlight the importance of Morse code in communication, security, rescue, and have attracted a lot of attention and researches [11, 12]. However, current Morse code transmitting devices are of rigid construction and lack the aesthetics and comfort of long-term wear. In addition,

Received: October 2, 2024; **Revised:** November 14, 2024
Accepted: December 2, 2024

✉Address correspondence to Zhong Lin Wang, zlwang@gatech.edu; Tao Jiang, jiangtao@binn.cas.cn; Hai-Dong Yu, iamhdyu@nwpu.edu.cn

they are usually dependent on external power for operations which are large in size, limiting the development of Morse code devices [13–15]. With the deepening of human-computer interaction, the amount of information generated increases, and the single function of the traditional Morse code transmitter cannot meet the needs of this diverse information.

Recently, many research studies have been dedicated to integrating flexible electronic technology with Morse code transmitting equipment, which provides more possibilities for convenient and accurate transmission of Morse code. For example, researchers use wearable pressure sensors [16, 17], humidity sensors [18, 19], etc. for Morse code transmission, which greatly reduces the size of the Morse code transmitter but still requires an external device to power it. At the same time, some self-supplied Morse code transmitters can only transmit raw Morse code signals without post-processing these signals, which cannot meet the needs of practical intelligent applications [20, 21]. A potential solution is to offer a wearable device with low-cost, lightweight, high flexibility, conformal energy-harvesting, and intelligent identification ability. Such a device can be continuously self-powered using either ambient energy or energy generated by human movement. This not only enhances the durability and reliability of the device but also meets the need for wearable comfort. Fortunately, triboelectric nanogenerator (TENG) is considered as an epoch-making energy harvesting technology, and intensive progress has been made in micro- and nano-energy harvesting [22–24], self-powered sensors [25–28], and blue energy harvesting [29–31]. The TENG offers several advantages including high electrical outputs, microscale motion detection, and the ability to monitor weak physiological signals from the human body [32–35]. Recently, researchers have found that TENGs also possess a huge potential in harvesting tiny energies, such as finger tapping. For the merits of high sensitivity, self-powered operation, and response to pressure, TENG is an effective strategy for preparing Morse code transmitters. However, achieving high sensitivity and lightweight at the same time is a great challenge. In addition, existing TENG-based wearable Morse code transmitters lacks deep human-computer interaction abilities, such as sensing and transforming finger-tapping signals, which significantly hinders their applications [36, 37]. Therefore, the TENG as a wearable Morse code transmitting device is subject to further researches. Silk fibroin, known for its excellent electropositive properties and biocompatibility, not only enhances the triboelectric performance of the device but also ensures its environmental friendliness, making it particularly suitable for wearable and portable TENG devices. Compared to synthetic polymers commonly used in TENGs, such as polyvinylidene fluoride (PVDF), polytetrafluoroethylene (PTFE), and nylon, the silk fibroin is more cost-effective and eco-friendly, which are urgent needs for wearable and portable applications in real-world environments [38–40]. In China, the researches primarily focus on material modification, device design, and output performance enhancement [41–43]. However, there remain opportunities for further advancements in achieving stable multifunctional integration and expanding the scope of applications. International researches emphasize the biocompatibility, especially in multifunctional sensing and flexible energy applications [44, 45]. However, further progress is needed in environmental adaptability, system integration, and device intelligence.

Herein, we report a versatile and convenient method to prepare a sandwich-structured silk fibroin fibers-based triboelectric nanogenerator. Due to the excellent electropositive property of silk fibroin, the silk fibroin fibers-based triboelectric nanogenerator (SF-TENG) can achieve an open-circuit voltage (V_{OC}) of 35 V, a short-circuit current (I_{SC}) of 60 nA, and a power density of 1.0 mW·m^{-2} at a contact area of 3 cm × 3 cm and an external force of 10 N. To meet the application of real-time conversion of tapping signals into Morse code and translation into letters, we combine the SF-TENG with optimized artificial intelligence (AI) algorithms to achieve real-time Morse code-to-letter conversion, which can obtain a high recognition accuracy of 96.67%. It can be predictable that this SF-TENG has broad application prospects in outdoor sports, silent encrypted signal communication, and robotic AI.

2 Results and discussion

2.1 Fabrication of the SF-TENG and characterization

The device can be used for SOS signal transmission in mountaineering and silent signal transmission in the animal protection field. Figure 1(a) shows the basic structure of the single-electrode mode SF-TENG assembled by nanocomposite membranes. The diagram clearly shows how the SF-TENG is flexibly attached to the fingertip, converting the small kinetic energy of the fingertip touch into electrical signals. We have characterized the surface of the friction layer of SF-TENG, whose scanning electron microscopy (SEM) image is shown in the top-right corner of Fig. 1(a), showing that the filament protein fibers exhibit a uniform distribution. The SF-TENG employs laser-cut silk fibroin membranes with various sizes and shapes, enabling adaptation to larger surfaces and diverse wearable applications. By adjusting layer dimensions or silk fibroin mass fraction, the device can achieve higher output, making it suitable for applications in body-area sensing, large-area touch interfaces, and environmental monitoring. Figure 1(b) illustrates the preparation process of SF-TENG. Firstly, we prepared SF nanofibrous membranes by electrostatic spinning technology. The electrostatic spinning equipment consists of three parts: a high-voltage power supply, a syringe with a metal needle, and a collector. Secondly, to obtain a flexible and thin TENG electrode layer, we used the magnetron sputtering technique to coat the surface of the SF fiber membrane with a Ag coating. In this process, magnetron sputtering was conducted with high-purity metallic silver at a power of 50 W for 600 s. The sample stage was rotated at a speed of 40 r·min^{-1} to ensure uniform attachment of silver particles on the nanofiber surface. This setup resulted in a silver layer with an approximate thickness of 100 nm. As can be seen from Fig. S1 in the Electronic Supplementary Material (ESM), when the magnetron sputtering power is 50 W, the SF spun fiber membranes before and after magnetron sputtering show one diffuse bun peak in the range of 10°–30°, which corresponds to the amorphous peak of SF fiber membranes. The four diffraction peaks at 2θ of 38.2°, 44.4°, 64.6°, and 77.6° of the SF spun fiber membrane before and after magnetron sputtering correspond to the (111), (200), (220), and (311) crystal planes of silver, which indicates that the magnetron sputtering builds up Ag particles with a certain energy and nucleation density on the surface of SF spun fiber membrane. This step ensures that the conductive layer has a very low resistivity while meeting the flexibility and air permeability. The SF-TENG presents an overall sandwich structure: The bottom layer is a breathable tape to protect the electrodes from moisture erosion, the middle layer is a single-sided magnetron sputtered silver-coated

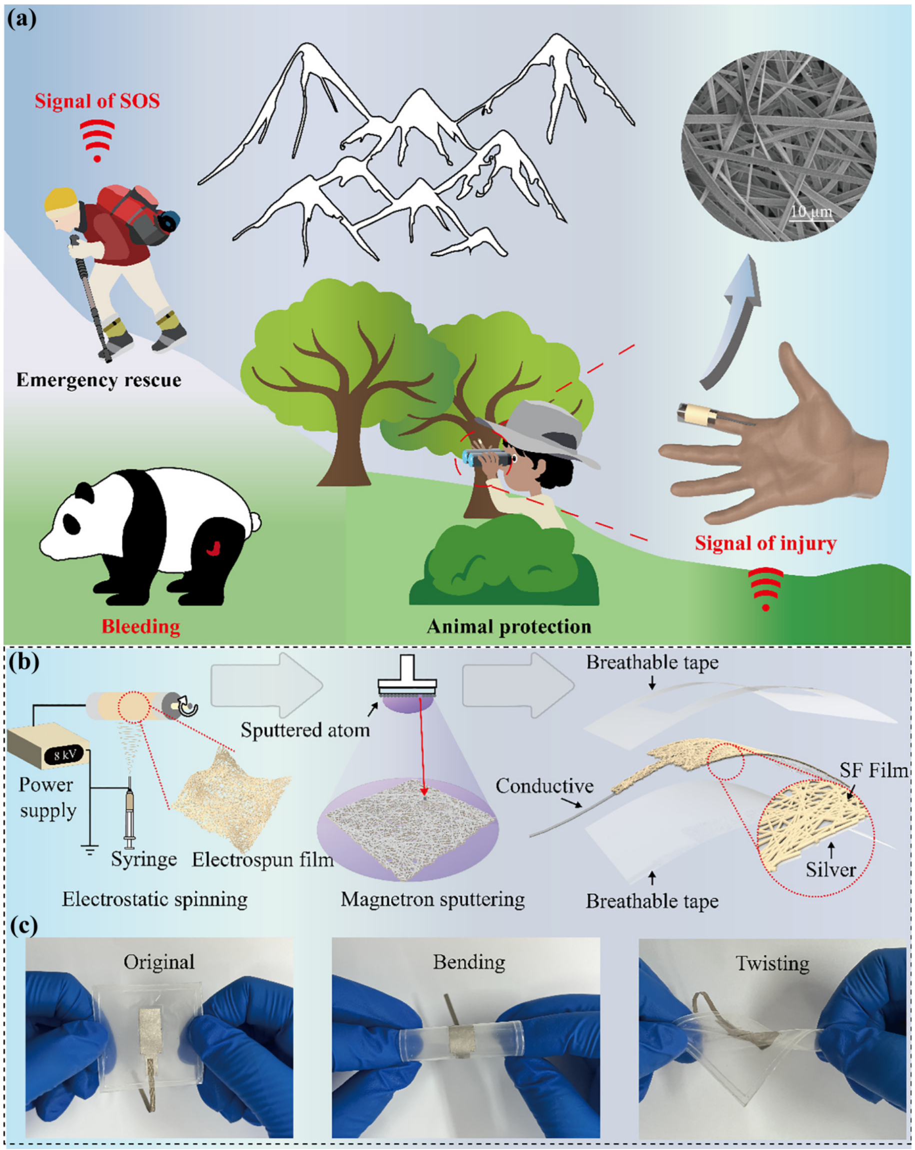

Figure 1 Application scenarios and fabrication of the SF-TENG. (a) Schematic illustration of the application scenarios of the SF-TENG and SEM image of the SF surface. (b) Illustration of the fabrication process of the SF-TENG. (c) Optical images of the bending and twisting of the SF-TENG.

SF fiber membrane, and the top layer is a laser-cut breathable tape which allows the SF fiber membrane to be partially exposed. The SF fiber membrane acts as a friction layer and the magnetron sputtered silver-coated layer is the conductive layer of the TENG. In addition, the SF-TENG includes a tail comprising a laser-cut conductive fabric connected to the magnetron sputtered silver plating of the SF-TENG by a conductive silver paste to facilitate the transfer of the charges accumulated by the SF-TENG. The SF-TENG is made of the green silky egg fiber membrane as a friction layer, which, due to its good biocompatibility, excellent flexibility, and a strong tendency to acquire electrons, allows it to generate triboelectric charges with external objects. Magnetron sputtered silver thin films were uniformly distributed in the SF nanofiber network, which act as flexible electrodes to stabilize the SF-TENG under different degrees of deformation. The experimental section describes in detail the preparation process of microstructured SF-TENG. Since all materials of SF-TENG are flexible, thin, and breathable, and have good mechanical properties, they can support a variety of complex mechanical deformations, including torsion and bending (Fig. 1(c)). In addition, these materials contribute to the thin thickness and light weight of the entire device, with the SF-TENG being only 0.3 mm thick and weighing 354 mg (with an area of 4.5 cm × 4.5 cm; Fig. S2 in the ESM shows the details).

2.2 Working mechanism and output performance

To test the working mechanism and output performance of SF-TENG, we assembled a test platform on a linear motor. The schematic diagram of the test platform and device is shown in Fig. 2(a). In our tests, we used the SF nanofiber films containing magnetron-sputtered silver-backed electrodes and PTFE films as the tribo-pair with a contact area of 9 cm^2. By adjusting the operating cycles of the linear motor, we investigated the output performance of the SF-TENG. The specific working principle of SF-TENG is shown in Fig. 2(b), which adopts the coupling of triboelectrification and electrostatic induction. When the SF nanofiber film and PTFE film come into contact under a pressure, the PTFE film gains electrons and becomes negatively charged, while the SF film loses electrons and becomes positively charged.

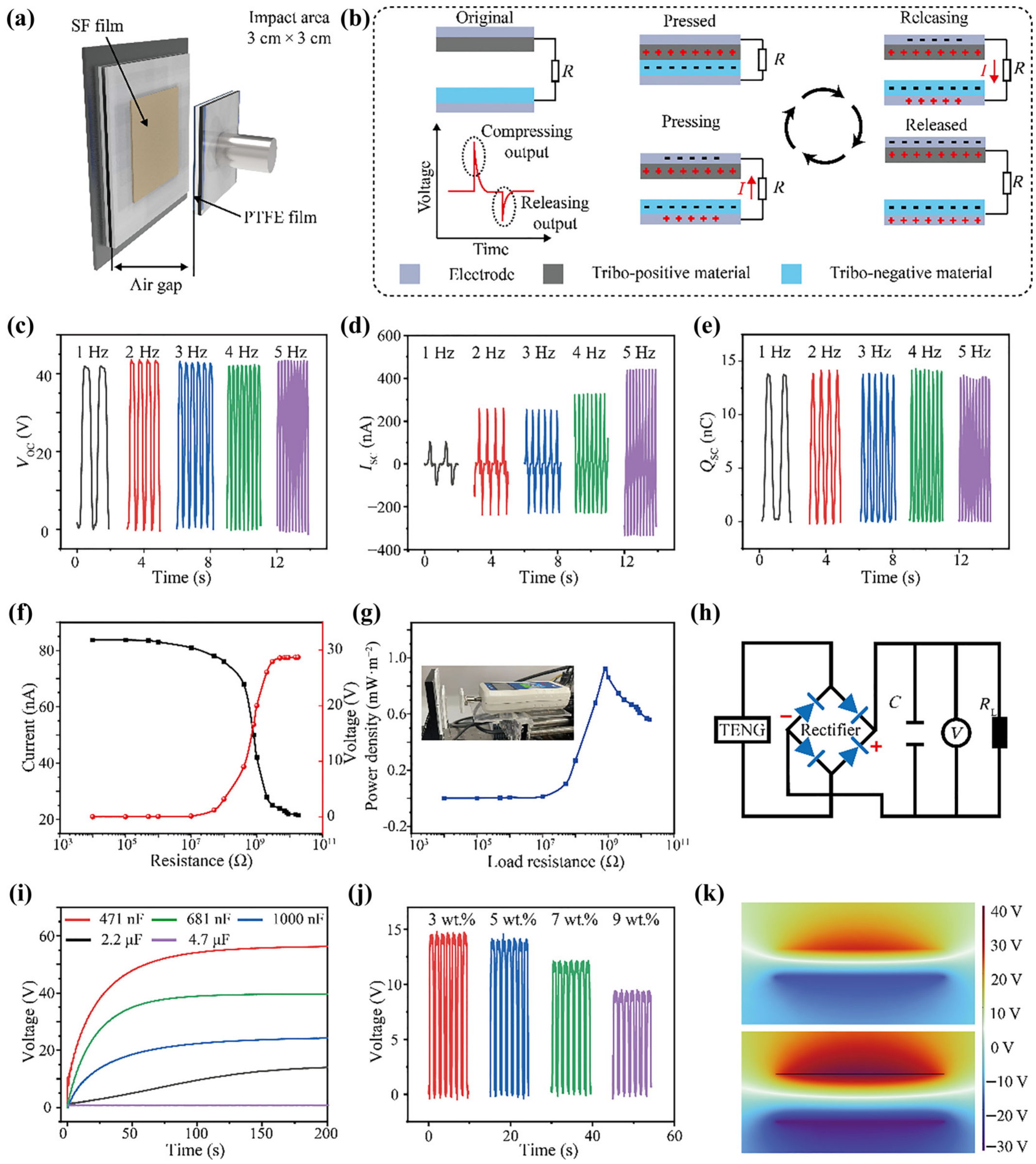

Figure 2 Working mechanisms and output performance of the SF-TENG. (a) Schematic illustration of the testing mode of the SF-TENG. (b) Schematics of the operating principle for the SF-TENG. (c)–(e) V_{OC}, I_{SC}, and Q_{SC} of the SF-TENG under different frequencies (1–5 Hz). (f) and (g) Output voltage, output current, and output power density of the SF-TENG under variable load resistances. (h) Schematic illustration of the rectifying circuit for energy storage. (i) Charging curves of the TENG to different capacitors. (j) Output voltage of the TENGs based on SF fiber membranes with different mass fractions. (k) Potential distribution of the SF-TENG simulated by COMSOL.

When the pressure is gradually released, the separation of opposite charges creates a potential difference between the two electrodes, driving the electrons to flow from the bottom electrode to the top electrode. After the maximum separation, when the TENG is subjected to an external force again, the approaching of two tribo-surfaces breaks the electrostatic balance and causes the electrons to flow back to the bottom electrode from the top electrode. During the periodic contact-separation process, alternative output current is generated across the load.

In the experiments, we chose a contact area of 3 cm × 3 cm, applied a force of 10 N, and set the maximum moving distance to be 50 mm. The output performance of the SF-TENG at different frequencies ranging from 1 to 5 Hz was compared. Figures 2(c) and 2(e) show that the open-circuit voltage (V_{OC}) and short-circuit transferred charge (Q_{SC}) exhibit no noticeable variations with increasing the frequency, which are both determined by the triboelectric charge density. By contrast, the I_{SC} increases obviously with the frequency, as shown in Fig. 2(d). Then the loading resistive behavior of the SF-TENG was measured, showing that the maximum output current decreases as the external resistance increases, but the output voltage increases (Fig. 2(f)). The TENG can deliver a peak power density of 1.0 mW·m^{-2} at the matched resistance of 1 GΩ (Fig. 2(g)). Moreover, the power generated by the SF-TENG can be rectified and stored in a capacitor or a battery for further use, and the equivalent circuit is shown in Fig. 2(h). Figure 2(i) further demonstrates the charging performance of SF-TENG at different capacitances, indicating that the charging rate is accelerated as the capacitance decreases. In addition, we prepared the SF-TENGs with different mass fractions and observed the nanofiber structures by the SEM (Fig. S3 in the ESM). After a comprehensive comparison, we chose the SF fibrous film of 7% mass fraction as the triboelectric layer of SF-TENG. Compared with the polyamide (PA) film, the SF film prepared using electrostatic spinning has a nanofiber network structure which has a larger specific surface and a rough surface, and these properties are more conducive to the TENG performance (Fig. S4 in the ESM). With the increase of the mass fraction, the diameter of nanofibers in SF-TENG gradually increases, and the output voltage gradually decreases (Fig. 2(j)). Further, by the finite element simulations using COMSOL software, we investigated the electrical potential distributions of SF fiber membranes and PTFE films during the contact separation motion (Fig. 2(k)).

2.3 Sensing characterization

Due to its excellent pressure sensing performance, the SF-TENG shows potential applications in self-powered human-computer interaction devices. Figure 3(a) reveals two distinct pressure sensitivity regions in the SF-TENG device. In the low-pressure region (0–25 kPa), the SF-TENG demonstrates a linear response with a pressure sensitivity of 1.767 mV·Pa^{-1}, attributed to a larger incremental contact area as the pressure increases. In the high-pressure region (25–40 kPa), the sensitivity decreases to 0.315 mV·Pa^{-1}, reflecting a smaller incremental contact area. The maximum pressure detection range is up to 40 kPa, beyond which the device is susceptible to damage. This segmented sensitivity range provides insight into the SF-TENG's behavior across different pressures, enhancing its applicability for a range of tactile sensing applications. The long-term stability of the TENG is essential for its practical applications, especially for repeated and real-time mechanical activity. The V_{OC} was measured for nearly 2000 cycles under optimal conditions, as demonstrated in Fig. 3(b). Additionally, it is important to consider environmental factors such as humidity and temperature, which may influence the long-term performance. High humidity can lead to increased charge dissipation, potentially resulting in reduction of output voltage and current. Thus, in practical applications, optimizing the environmental conditions could further enhance the reliability and stability of the SF-TENG in diverse settings. As shown in Table S1 in the ESM [46–50], the SF-TENG's pressure sensitivity in the 0–25 kPa range is notably higher than that of other materials like deposited Cu film and graphene, highlighting its advantage in precise pressure sensing applications. Figure 3(c) shows that the output voltage increases as the applied contact force increases, eventually reaching saturation at 62 V as the force approaches 35 N (the pressure is 40 kPa). This result can be attributed to the fact that the applied pressure increases the contact area and the surface charge density, producing a higher voltage output. The tendencies of the I_{SC} and Q_{SC} with the applied contact force are similar (Figs. 3(d) and 3(e)). Based on the SF-TENG's stable and sensitive performance, we developed a Morse code acquisition and

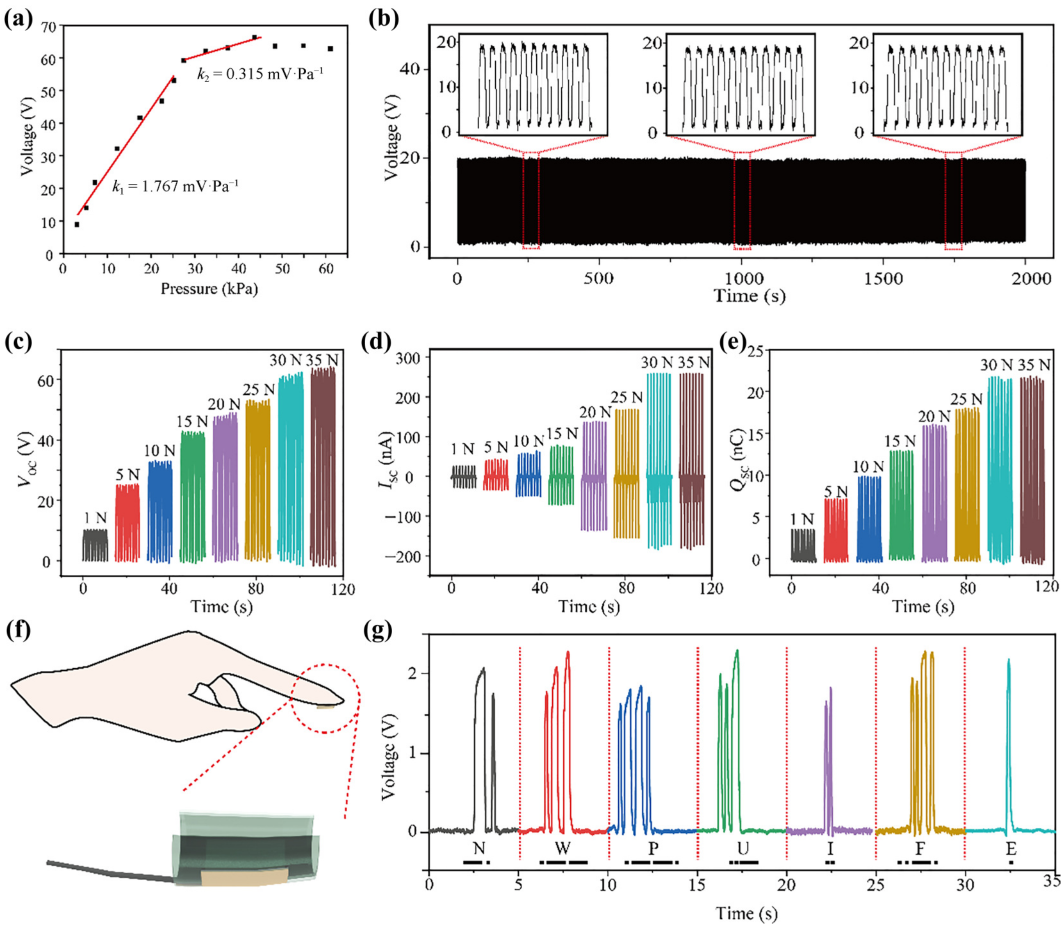

Figure 3 Electrical outputs, stability, and sensitivity of the SF-TENG. (a) Output voltage of the SF-TENG in response to the applied pressure. (b) Varying trend of V_{OC} of the SF-TENG during 2000 cycles. (c)–(e) V_{OC}, Q_{SC}, and I_{SC} of the SF-TENG under different pressures (under the applied force of 10 N and the loading frequency of 1 Hz, the V_{OC} of up to 35 V and an I_{SC} of 60 nA). (f) Schematic of the wearable SF-TENG for Morse signal output. (g) Output voltage signals of different letters based on the SF-TENG.

conversion system. To handle noise, we applied threshold-based filtering and time-domain analysis, ensuring accurate decoding by distinguishing intentional inputs from interference. Morse code is a system used for communication that relies on a series of dots and scratches to convey coded information. In order to output the Morse code signal, we wore the SF-TENG at the index finger to signal the 26 letters (Fig. S5 in the ESM), as shown schematically in Fig. 3(f). We performed the acquisition of the tapping signals for the letters N, W, P, U, I, F, and E. The voltage signals obtained are shown in Fig. 3(g), where the dots and dashes correspond to the short and long presses of the SF-TENG signals (the duration of short pressure is about 0.2 s, and the duration of long pressure is about 0.75 s). The graph clearly shows the peaks of the voltage signals of the different letters. By analyzing the peaks, the SF-TENG signals can be converted to the corresponding letters in real time.

2.4 Application in the real-time detection and translation of Morse code

Morse code transmitters play a key role in information and communication equipment and are especially vital in security applications. Through its lightweight and flexible design, the SF-TENG is able to harvest the tiny energy of fingertip tapping and convert it into electrical signals that can be used to send Morse code. This design not only helps humans work and stay safe in areas such as outdoor adventure and animal tracking and protection, but also increases the wearer's experience, making the communication devices more comfortable and convenient. In order to extend the application of the wearable SF-TENG device as a Morse code transmitter in real-time, we can improve the SF-TENG based on deep learning capabilities. In this way, the SF-TENG converts the energy of fingertip tapping into electrical signals, enabling real-time transmission of Morse code. This innovation creates new application scenarios for real-time transmission of Morse code, making it more widely applicable in the field of communications.

The process flow of Morse code from the SF-TENG information acquisition to real-time prediction is shown in Fig. 4(a). Firstly, when the user uses the SF-TENG, the resulting electrical output signal is converted to a digital signal by the NI USB-6356 acquisition card and 6517B electrometer and decoded using the LabView program. After the signal filtering and conversion process, the real-time digital signal is transmitted to the computer and displayed in the software program. Through a specially designed program, the real-time knockout voltage waveform graph of SF-TENG as well as the predicted Morse code signals and predicted letters can be presented in real time on the computer interface. Figure 4(b) shows the schematic diagram of the Morse code identification and communication system. The complete real-time control system consists of the SF-TENG, the signal NI USB-6363 acquisition card and 6517B electrometer, the PC, and the virtual space in the Thinter software. For practical applications, a sensing system of Morse code transmitters was developed through integrating the SF-TENG with a human-machine interface. The data collection with machine learning ensured that the model could

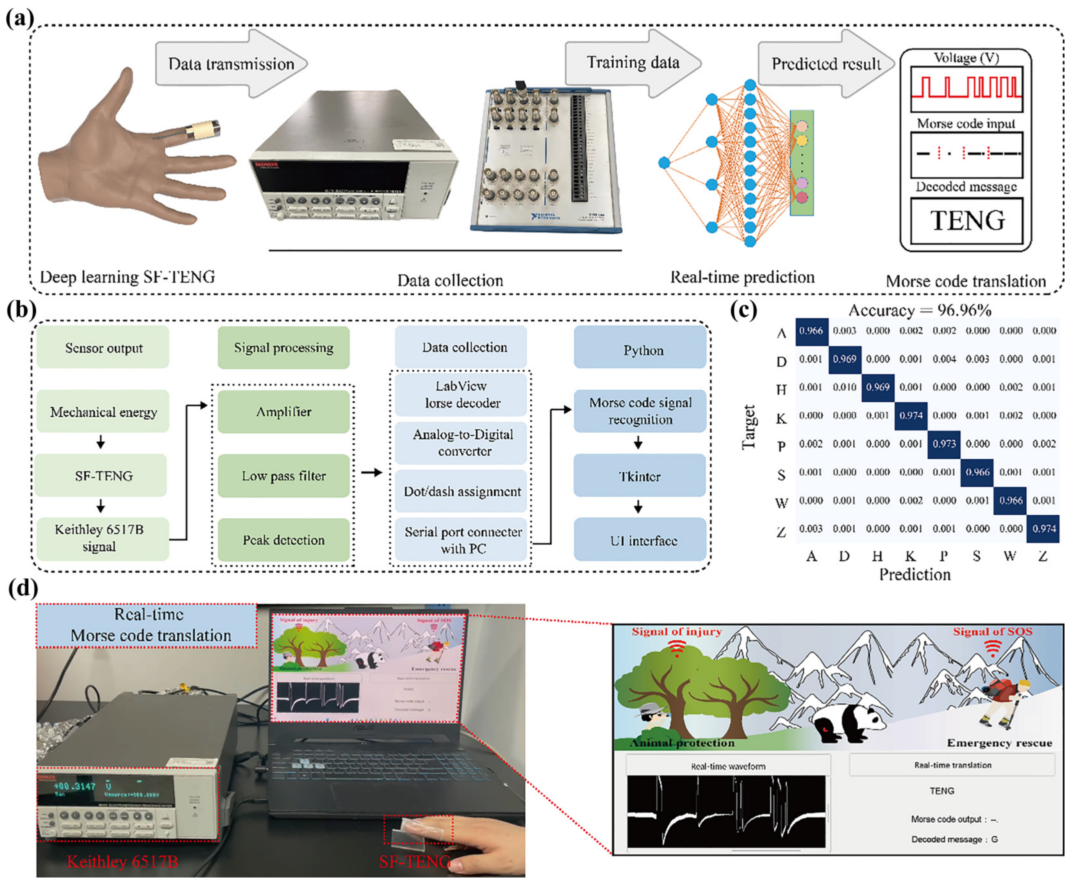

Figure 4 Applications of the SF-TENG for Morse code translation. (a) The process flow from the SF-TENG information collection to the real-time prediction in Morse code translation. (b) Schematic diagram of the Morse code recognition and communication system. (c) Confusion map of split word element recognition (accuracy 96.96%). (d) Demonstration showing that the SF-TENG controls Morse code translation.

effectively capture and distinguish subtle variations in signal patterns generated by the SF-TENG from a single user. Futhermore, using data from multiple users with varying tapping strengths could further test the model's robustness. Future work may incorporate data from multiple users to further enhance the model's generalizability and adaptability across different tapping styles, aligning with our goal of developing a universally applicable Morse code recognition system. Based on the received signal spectrum, the machine learning model processes the Morse code inputs and outputs the corresponding letters. The model, as shown in Fig. S6 in the ESM, was trained with 100 samples per letter, achieving an average recognition accuracy of 96.67% across all 26 letters and an average recognition time of below 500 ms per letter, underscoring its real-time performance capabilities. Figure 4(c) illustrates the confusion matrix for a subset of letters, specifically showcasing recognition accuracy for the letters A, D, H, K, P, S, W, and Z, with an average accuracy reaching 96.96%. Additionally, Figs. S7 and S8 in the ESM provide further insights into the model's training process. Figure S7 in the ESM displays the iteration accuracy across the process, showing steady improvement and high accuracy in letter recognition. Figure S8 in the ESM shows the loss rates for both training and validation data, which decrease rapidly in the initial stage and stabilize, indicating effective model convergence. These results validate the SF-TENG's reliable performance in accurate Morse code recognition. Figure 4(d) and Movie S1 in the ESM demonstrate an application of real-time reception and translation of Morse code based on SF-TENG. It can be found that the SF-TENG can be easily worn on the finger, and the small energy generated by finger tapping can be quickly converted into words outputted in the window. Therefore, the SF-TENG has the characteristics of ultra-thinness, flexibility, and high sensitivity, and exhibits wide potential application prospects in the fields of human-machine interfaces, human micro-energy harvesting, and security systems.

3 Conclusions

In summary, we have successfully designed a lightweight, flexible, and highly sensitive SF-TENG based on SF fibers and magnetron-sputtered silver electrodes. The total thickness of this device is only about 0.3 mm and the weight is only 354 mg, which greatly reduces the burden of conventional Morse code collection devices. The SF-TENG exhibits excellent stability and flexibility, allowing it to easily attach to human fingertips for energy harvesting and signal sensing while ensuring comfort. Under an external force of 10 N and a loading frequency of 1 Hz, the SF-TENG can achieve a V_{OC} of up to 35 V and an I_{SC} of 60 nA, respectively, proving that it can provide stable output performance in various environments. In addition, the SF-TENG achieves a high pressure sensitivity of 1.767 $mV \cdot Pa^{-1}$ within the low-pressure range of up to 0–25 kPa, enabling it to effectively sense subtle pressure changes. Furthermore, we designed and demonstrated a self-powered Morse code transmitter capable of real-time Morse code translation, achieving an accuracy of 96.67% through a machine learning model. To ensure accurate recognition, we employed data preprocessing techniques that emphasized distinct voltage changes at the start and end of signals and applied boundary threshold processing, allowing the model to differentiate subtle variations even between similar signals. This robust approach enhances the transmitter's reliability in real-world applications. Considering the SF-TENG's significant advantages in terms of thickness, weight, and pressure sensitivity, it holds great promise for both self-powered sensing and energy providing for the next generation of wearable electronics.

4 Experimental section

Preparation of nanofiber films: Water-soluble filipin protein feedstock was dissolved in hexafluoroisopropanol (HFIP) solution at a concentration of 7 wt.%. After 12 h of magnetic stirring at 1000 rpm at room temperature, the SF spinning solution was poured into a 10 mL plastic syringe. The electrostatic spinning process was carried out at a positive voltage of 8 kV and a negative voltage of 2 kV, and the distance between the needle and the collector was set to be 20 cm. The pumping rate for SF electrostatic spinning was set at 0.5 $mL \cdot h^{-1}$. A release paper was coated on a rotating drum to collect the SF nanofiber film.

Magnetron sputtering: The prepared SF nanofiber film was fixed on a magnetron sputtering sample disc and magnetron sputtered for 600 s at 50 W. A layer of silver with a thickness of 100 nm was coated on the SF surface by magnetron sputtering. A laser cutter was used to cut the magnetron-sputtered SF nanofiber film, medical breathable tape, and conductive cloth into suitable sizes for assembling into the SF-TENG.

Characterization and measurement: The surface morphologies of the samples with nanofiber structures were characterized using a SU8020 cold-field scanning electron microscopy. X-ray diffraction (XRD) analysis of SF, as well as SF after magnetron sputtering Ag plating, was tested using Xpert3 Powder.

Electrical performance tests: A stepper motor (Linmot E1100) was used to provide regular contact-separation motion for the SF-TENG. The V_{OC}, I_{SC}, and Q_{SC} were tested using an acquisition card (USB-6356) with a Keithley 6517B electrometer. A software platform was constructed based on LabView to realize real-time data acquisition.

Signal processing method: The knocking signals were converted by the SF-TENG, and the sound signals with extracted feature values were trained by Tkinter to form a classification network. Finally, the classification network was used to classify and identify the real-time knocking signals.

Electronic Supplementary Material: Supplementary material (including XRD patterns, machine learning model training details, and further characterization of SF-TENG performance) is available in the online version of this article at https://doi.org/10.26599/NR.2025.94907167.

Data availability

All data needed to support the conclusions in the paper are presented in the manuscript and the Electronic Supplementary Material. Additional data related to this paper may be requested from the corresponding author upon request.

Acknowledgments

The authors thank the National Key R&D Project from Minister of Science and Technology (Nos. 2021YFA1201604 and 2021YFA1201601), the China National Postdoctoral Program for Innovative Talents (No. BX20230357), Project supported by the Fundamental Research Funds for the Central Universities (No. E3E46807X2), the China Postdoctoral Science Foundation (No.

2023M743445), the National Key R&D Program of China (No. 2023YFB2604600), and the National Natural Science Foundation of China (No. 52302115).

Declaration of competing interest

The authors declare no competing financial interest. Author Zhong Lin Wang is the advisory board member of this journal, but he is not involved in the peer-review or decision of this article.

Author contribution statement

S. X. T.: Data curation, project administration, validation, writing manuscript, experimental design. Y. J.: Data curation, project administration, validation, experimental design. X. J. C.: Project administration, writing manuscript. F. L.: Project administration, writing manuscript. R. P. L.: Machine learning, investigation, validation. T. J.: Supervision, validation, writing – review & editing, revising. H.-D. Y.: Supervision, validation, writing – review & editing, revising. Z. L. W.: Supervision, validation, writing – review & editing, revising. All the authors have approved the final manuscript.

Use of AI statement

None.

References

[1] Zhang, Y. F.; Fu, J. J.; Ding, Y. C.; Babar, A. A.; Song, X.; Chen, F.; Yu, X. G.; Zheng, Z. J. Thermal and moisture managing E-textiles enabled by Janus hierarchical gradient honeycombs. *Adv. Mater.* **2024**, *36*, 2311633.

[2] An, Z. J.; Fu, Q. Q.; Lv, J. J.; Zhou, T.; Wu, Y.; Lu, Y. L.; Liu, G.; Shi, Z. H.; Li, X.; Zhang, F. N. et al. Body heat powered wirelessly wearable system for real-time physiological and biochemical monitoring. *Adv. Funct. Mater.* **2023**, *33*, 2303361.

[3] Zhang, Q. X.; Lei, D. D.; Liu, N. S.; Liu, Z. Y.; Ren, Z. Q.; Yin, J. Y.; Jia, P. X.; Lu, W. Z.; Gao, Y. H. A zinc-ion battery-type self-powered pressure sensor with long service life. *Adv. Mater.* **2022**, *34*, 2205369.

[4] Chao, M. Y.; Di, P. J.; Yuan, Y.; Xu, Y. J.; Zhang, L. Q.; Wan, P. B. Flexible breathable photothermal-therapy epidermic sensor with MXene for ultrasensitive wearable human-machine interaction. *Nano Energy* **2023**, *108*, 108201.

[5] Guo, P. W.; Tian, B.; Liang, J.; Yang, X. P.; Tang, G. L.; Li, Q. C.; Liu, Q.; Zheng, K.; Chen, X.; Wu, W. An all-printed, fast-response flexible humidity sensor based on hexagonal-WO_3 nanowires for multifunctional applications. *Adv. Mater.* **2023**, *35*, 2304420.

[6] Chen, X. P.; Luo, F.; Yuan, M.; Xie, D. L.; Shen, L.; Zheng, K.; Wang, Z. P.; Li, X. D.; Tao, L. Q. A dual-functional graphene-based self-alarm health-monitoring E-skin. *Adv. Funct. Mater.* **2019**, *29*, 1904706.

[7] Li, L. L.; Wang, D. P.; Zhang, D.; Ran, W. H.; Yan, Y. X.; Li, Z. X.; Wang, L. L.; Shen, G. Z. Near-infrared light triggered self-powered mechano-optical communication system using wearable photodetector textile. *Adv. Funct. Mater.* **2021**, *31*, 2104782.

[8] Fang, D.; Ding, S.; Dai, Z. Y.; Zhong, J. W.; Zhou, B. P. Wearable patch with direction-aware sensitivity of in-plane force for self-powered and single communication channel based human-machine interaction. *Chem. Eng. J.* **2023**, *468*, 143664.

[9] Galli, V.; Sailapu, S. K.; Cuthbert, T. J.; Ahmadizadeh, C.; Hannigan, B. C.; Menon, C. Passive and wireless all-textile wearable sensor system. *Adv. Sci.* **2023**, *10*, 2206665.

[10] Kim, J. H.; Marcus, C.; Ono, R.; Sadat, D.; Mirzazadeh, A.; Jens, M.; Fernandez, S.; Zheng, S. Q.; Durak, T.; Dagdeviren, C. A conformable sensory face mask for decoding biological and environmental signals. *Nat. Electron.* **2022**, *5*, 794–807.

[11] Cao, Y.; Yang, Y.; Qu, X. C.; Shi, B. J.; Xu, L. L.; Xue, J. T.; Wang, C.; Bai, Y.; Gai, Y. S.; Luo, D. et al. A self-powered triboelectric hybrid coder for human-machine interaction. *Small Methods* **2022**, *6*, 2101529.

[12] Sun, M. M.; Xiang, X. P.; Qin, H. Y.; Li, P. Y.; Li, Y. X.; Zhao, J. X.; Zhai, X. J.; Wu, L. D. Polydopamine-triggered adhesive and conductive hydrogel for Morse code communication at polar environments. *Sens. Actuators A: Phys.* **2023**, *364*, 114813.

[13] Gong, T.; Jia, J.; Sun, X. R.; Li, W. D.; Ke, K.; Bao, R. Y.; Yang, W. Design strategy for hierarchical structure of carbon black on microporous elastomer surface toward stretchable and compressive strain sensors. *Carbon* **2023**, *206*, 53–61.

[14] Gu, Y. F.; Hao, J. Y.; Wu, T. C.; Zhang, Z. G.; Zhang, Z. X.; Li, Q. H. Bimetallic MoNi/WNi nanoalloys for ultra-sensitive wearable temperature sensors. *J. Mater. Chem. A* **2022**, *10*, 5402–5409.

[15] Di, X.; Hou, J. W.; Yang, M. M.; Wu, G. L.; Sun, P. C. A bio-inspired, ultra-tough, high-sensitivity, and anti-swelling conductive hydrogel strain sensor for motion detection and information transmission. *Mater. Horiz.* **2022**, *9*, 3057–3069.

[16] Adepu, V.; Tathacharya, M.; Cs, R.; Mattela, V.; Sahatiya, P. TeNWs/$Ti_3C_2T_x$ Nanohybrid-based flexible pressure sensors for personal safety applications using morse code. *ACS Appl. Nano Mater.* **2022**, *5*, 18209–18219.

[17] Sun, X. L.; He, Q. Q.; Hou, Y.; Zheng, X.; Bi, P.; Xu, Y. F.; Zhang, X. Z.; Liu, Y.; Xiong, R.; Yang, Y. et al. Self-healing flexible pressure sensor for human motion detection based on silver-nanoparticle-modified polyimide membranes. *ACS Appl. Polym. Mater.* **2023**, *5*, 5951–5960.

[18] Tang, M. C.; Liu, X. H.; Zhang, D. Z.; Zhang, H.; Xi, G. S. Ultra-sensitive humidity QCM sensor based on sodium alginate/polyacrylonitrile composite film for contactless Morse code communication. *Sens. Actuators B: Chem.* **2024**, *407*, 135429.

[19] Liu, H.; Qin, J. X.; Yang, X. G.; Lv, C. F.; Huang, W. T.; Li, F. K.; Zhang, C.; Wu, Y. R.; Dong, L.; Shan, C. X. Highly sensitive humidity sensors based on hexagonal boron nitride nanosheets for contactless sensing. *Nano Res.* **2023**, *16*, 10279–10286.

[20] Wang, Z. S.; Wan, D.; Fang, R.; Yuan, Z. Y.; Zhuo, K.; Wang, T.; Zhang, H. L. Water-based triboelectric nanogenerator for wireless energy transmission and self-powered communication via a solid-liquid-solid interaction. *Appl. Surf. Sci.* **2022**, *605*, 154765.

[21] Bagchi, B.; Datta, P.; Fernandez, C. S.; Gupta, P.; Jaufuraully, S.; David, A. L.; Siassakos, D.; Desjardins, A.; Tiwari, M. K. Flexible triboelectric nanogenerators using transparent copper nanowire electrodes: Energy harvesting, sensing human activities and material recognition. *Mater. Horiz.* **2023**, *10*, 3124–3134.

[22] Sun, Q. Z.; Ren, G. Z.; He, S. H.; Tang, B.; Li, Y. J.; Wei, Y. W.; Shi, X. W.; Tan, S. X.; Yan, R.; Wang, K. L. et al. Charge dispersion strategy for high-performance and rain-proof triboelectric nanogenerator. *Adv. Mater.* **2024**, *36*, 2307918.

[23] Sun, Q. Z.; Liang, F.; Ren, G. Z.; Zhang, L. R.; He, S. H.; Gao, K.; Gong, Z. Y.; Zhang, Y. L.; Kang, X.; Zhu, C. C. et al. Density-of-states matching-induced ultrahigh current density and high-humidity resistance in a simply structured triboelectric nanogenerator. *Adv. Mater.* **2023**, *35*, 2210915.

[24] Zhao, H. F.; Wang, H.; Yu, H. Y.; Xu, Q. H.; Li, X. S.; Guo, J.; Shao, J. J.; Wang, Z. L.; Xu, M. Y.; Ding, W. B. Theoretical modeling of contact-separation mode triboelectric nanogenerators from initial charge distribution. *Energy Environ. Sci.* **2024**, *17*, 2228–2247.

[25] Yan, R.; Sun, Q. Z.; Shi, X. W.; Sun, Z. Q.; Tan, S. X.; Tang, B.; Chen, W. T.; Liang, F.; Yu, H. D.; Huang, W. Skin-interfaced self-powered pressure and strain sensors based on fish gelatin-based

hydrogel for wireless wound strain and human motion detection. *Nano Energy* **2023**, *118*, 108932.
[26] Jiang, Y.; Dong, K.; Li, X.; An, J.; Wu, D. Q.; Peng, X.; Yi, J.; Ning, C.; Cheng, R. W.; Yu, P. T. et al. Stretchable, washable, and ultrathin triboelectric nanogenerators as skin-like highly sensitive self-powered haptic sensors. *Adv. Funct. Mater.* **2021**, *31*, 2005584.
[27] Jiang, Y.; Zhang, Y. F.; Ning, C.; Ji, Q. Q.; Peng, X.; Dong, K.; Wang, Z. L. Ultrathin eardrum-inspired self-powered acoustic sensor for vocal synchronization recognition with the assistance of machine learning. *Small* **2022**, *18*, 2106960.
[28] Wu, H.; Wang, Z. H.; Zhu, B. Y.; Wang, H. Q.; Lu, C. Y.; Kang, M. C.; Kang, S. L.; Ding, W. B.; Yang, L. J.; Liao, R. J. et al. All-in-one sensing system for online vibration monitoring via IR wireless communication as driven by high-power TENG. *Adv. Energy Mater.* **2023**, *13*, 2300051.
[29] Hong, H. X.; Yang, X. Y.; Cui, H.; Zheng, D.; Wen, H. Y.; Huang, R. Y.; Liu, L. Q.; Duan, J. L.; Tang, Q. W. Self-powered seesaw structured spherical buoys based on a hybrid triboelectric-electromagnetic nanogenerator for sea surface wireless positioning. *Energy Environ. Sci.* **2022**, *15*, 621–632.
[30] Yang, S. H.; Zhang, C. Z.; Du, Z. C.; Tu, Y. Q.; Dai, X. G.; Huang, Y.; Fan, J. Y.; Hong, Z. Y.; Jiang, T.; Wang, Z. L. Fluid oscillation-driven Bi-directional air turbine triboelectric nanogenerator for ocean wave energy harvesting. *Adv. Energy Mater.* **2024**, *14*, 2304184.
[31] Ren, Z. W.; Liang, X.; Liu, D.; Li, X. J.; Ping, J. F.; Wang, Z. M.; Wang, Z. L. Water-wave driven route avoidance warning system for wireless ocean navigation. *Adv. Energy Mater.* **2021**, *11*, 2101116.
[32] Dong, X. Y.; Liu, Q.; Liu, S.; Wu, R. H.; Ma, L. Y. Silk fibroin based conductive film for multifunctional sensing and energy harvesting. *Adv. Fiber Mater.* **2022**, *4*, 885–893.
[33] Seifaddini, P.; Sheikhahmadi, S.; Kolahdouz, M.; Aghababa, H. Smart printed triboelectric wearable sensor with high performance for glove-based motion detection. *ACS Appl. Mater. Interfaces* **2024**, *16*, 9506–9516.
[34] Mi, H. Y.; Jing, X.; Zheng, Q. F.; Fang, L. M.; Huang, H. X.; Turng, L. S.; Gong, S. Q. High-performance flexible triboelectric nanogenerator based on porous aerogels and electrospun nanofibers for energy harvesting and sensitive self-powered sensing. *Nano Energy* **2018**, *48*, 327–336.
[35] Chen, S. W.; Cao, X.; Wang, N.; Ma, L.; Zhu, H. R.; Willander, M.; Jie, Y.; Wang, Z. L. An ultrathin flexible single-electrode triboelectric-nanogenerator for mechanical energy harvesting and instantaneous force sensing. *Adv. Energy Mater.* **2017**, *7*, 1601255.
[36] Qiu, H. J.; Song, W. Z.; Wang, X. X.; Zhang, J.; Fan, Z. Y.; Yu, M.; Ramakrishna, S.; Long, Y. Z. A calibration-free self-powered sensor for vital sign monitoring and finger tap communication based on wearable triboelectric nanogenerator. *Nano Energy* **2019**, *58*, 536–542.
[37] Chandrasekhar, A.; Vivekananthan, V.; Khandelwal, G.; Kim, S. J. A fully packed water-proof, humidity resistant triboelectric nanogenerator for transmitting Morse code. *Nano Energy* **2019**, *60*, 850–856.
[38] Xu, Z. J.; Qiu, W.; Fan, X. W.; Shi, Y. T.; Gong, H.; Huang, J. N.; Patil, A.; Li, X. Y.; Wang, S. T.; Lin, H. B. et al. Stretchable, stable, and degradable silk fibroin enabled by mesoscopic doping for finger motion triggered color/transmittance adjustment. *ACS Nano* **2021**, *15*, 12429–12437.
[39] Pang, C. L.; Li, F.; Hu, X. R.; Meng, K. Y.; Pan, H.; Xiang, Y. Degradable silk fibroin based piezoresistive sensor for wearable biomonitoring. *Discover Nano* **2024**, *19*, 55.
[40] DeBari, M. K.; King III, C. I.; Altgold, T. A.; Abbott, R. D. Silk fibroin as a green material. *ACS Biomater. Sci. Eng.* **2021**, *7*, 3530–3544.
[41] Li, Z. L.; Xu, S. X.; Xu, Z. J.; Shu, S.; Liu, G. L.; Zhou, J. D.; Lin, D.; Tang, W. Enhancing cellular behavior in repaired tissue via silk fibroin-integrated triboelectric nanogenerators. *Microsyst. Nanoeng.* **2024**, *10*, 68.
[42] Xiong, Q. H.; Yang, Z. H.; Zhang, X. H. Flexible triboelectric nanogenerator based on silk fibroin-modified carbon nanotube arrays. *Chem. Eng. J.* **2024**, *482*, 148986.
[43] Tan, X. Q.; Huang, Z. Y.; Pei, H. R.; Jia, Z. C.; Zheng, J. M. Highly porous, ultralight, biocompatible silk fibroin aerogel-based triboelectric nanogenerator. *ACS Sens.* **2024**, *9*, 3938–3946.
[44] Su, M.; Kim, B. Silk fibroin-carbon nanotube composites based fiber substrated wearable triboelectric nanogenerator. *ACS Appl. Nano Mater.* **2020**, *3*, 9759–9770.
[45] Dudem, B.; Dharmasena, R. D. I. G.; Graham, S. A.; Leem, J. W.; Patnam, H.; Mule, A. R.; Silva, S. R. P.; Yu, J. S. Exploring the theoretical and experimental optimization of high-performance triboelectric nanogenerators using microarchitectured silk cocoon films. *Nano Energy* **2020**, *74*, 104882.
[46] He, J. H.; Xie, Z. Q.; Yao, K. M.; Li, D. F.; Liu, Y. M.; Gao, Z.; Lu, W.; Chang, L. Q.; Yu, X. G. Trampoline inspired stretchable triboelectric nanogenerators as tactile sensors for epidermal electronics. *Nano Energy* **2021**, *81*, 105590.
[47] Kang, H.; Zhao, C. L.; Huang, J. R.; Ho, D. H.; Megra, Y. T.; Suk, J. W.; Sun, J.; Wang, Z. L.; Sun, Q.; Cho, J. H. Fingerprint-inspired conducting hierarchical wrinkles for energy-harvesting E-skin. *Adv. Funct. Mater.* **2019**, *29*, 1903580.
[48] Lee, Y.; Kim, J.; Jang, B.; Kim, S.; Sharma, B. K.; Kim, J. H.; Ahn, J. H. Graphene-based stretchable/wearable self-powered touch sensor. *Nano Energy* **2019**, *62*, 259–267.
[49] Wen, Z.; Yang, Y. Q.; Sun, N.; Li, G. F.; Liu, Y. N.; Chen, C.; Shi, J. H.; Xie, L. J.; Jiang, H. X.; Bao, D. Q. et al. A wrinkled PEDOT: PSS film based stretchable and transparent triboelectric nanogenerator for wearable energy harvesters and active motion sensors. *Adv. Funct. Mater.* **2018**, *28*, 1803684.
[50] Zhao, G. R.; Zhang, Y. W.; Shi, N.; Liu, Z. R.; Zhang, X. D.; Wu, M. Q.; Pan, C. F.; Liu, H. L.; Li, L. L.; Wang, Z. L. Transparent and stretchable triboelectric nanogenerator for self-powered tactile sensing. *Nano Energy* **2019**, *59*, 302–310.